Proof-of-Concept Simulations of The Magnetic Null (MagNul) Thruster

Matthew S. Feldman* and Edgar Y. Choueiri†

Electric Propulsion and Plasma Dynamics Laboratory, Princeton, New Jersey, 08544, USA

Plasma behavior in an externally applied magnetic field reversal is numerically explored in order to demonstrate the existence of a self-consistent drift caused by the kinetic interaction of ions with the magnetic null. Single-particle analysis of ion trajectories is performed in the magnetic topology to predict expected ion particle and momentum fluxes out of the system. A particle-in-cell (PIC) code is used to simulate the actual fluxes out of the system for a set of magnetic field strengths from 0 to 800 G. The results of the simulations upheld the concept's presumed ability to accelerate plasma in a desired direction and demonstrated that single-particle analysis does not predict the exact particle and momentum fluxes out of the system but does predict the optimum magnetic field for our limited parameter space.

Nomenclature

ω	Angular frequencies
ρ	Larmar radius
m	Mass
T	Temperature
B	Magnetic Field
A	Magnetic vector potential
δ	Magnetic null region size
q	Electric charge
t, τ	Time and normalized time
$P_{X,Y}$	Canonical momentum
h, H	Hamiltonian and normalized Hamiltonian
S	Normalize particle trajectory shape
v, u	Velocity and normalized velocity
x, y, X, Y	Position and normalized position
p	Momentum
R	Particle fill rate
n	Density
Subscript	
i, e	Ion, electron
c	Cyclotron
gc	Guiding Center of Cyclotron Motion
th	Thermal
d	Drift

*Graduate Student, Mechanical and Aerospace Engineering Department, Research Assistant.

†Chief Scientist, EPPDyL; Professor, Applied Physics Group; AIAA Fellow

I. Introduction

The Magnetic Null (MagNul) Thruster concept was recently proposed by Jorns and Choueiri[1] as a propulsion concept that relies on using beating electrostatic waves to stochastically heat ions and channel them towards a magnetic field reversal, where they are collectively directed to produce thrust. The thruster concept shown in Fig. 1 operates by launching electrostatic waves in the positive-$\hat{x}$ direction. These waves stochastically heat ions and channel them towards the reversed magnetic field, which tends to direct them in the forward, positive-$\hat{x}$ direction out of the thruster. The MagNul thruster has certain intrinsic advantages that deserve further study. The design is inherently steady state and electrodeless, which allows the thruster to avoid the lifetime limitations of electrodes. Beating waves can also be tuned to allow for variable specific impulse. Additionally, because the thrust mechanism occurs across magnetic field lines, the proposed device avoids traditional magnetic detachment issues, which can harm efficiency.

Previous work on ion acceleration and heating with beating electrostatic waves[4,6,7] has demonstrated that two electrostatic waves with a beat frequency equal to an integer multiple of the ion-cyclotron frequency can, under the right conditions, lead to a plasma energization that is significantly more efficient than is possible with a single wave. Unlike single electrostatic waves, these beating electrostatic waves can target a large fraction of the ion ensemble, which makes them ideal for directed ion acceleration. Gardineer et. al.[10] demonstrated, by numerically examining the single particle motion of ions in such a configuration, that beating waves are particularly well-suited for the magnetic null topology. These simulations of the ion dynamics suggested ion exhaust velocities on the order of at least 10km/s could be obtained for typical plasma and wave parameters currently used in laboratory experiments. Further study by Feldman and Choueiri[11] elucidated key requirements on the average ion and electron Larmor radii and the length scale of the magnetic field reversal, δ. In particular, Feldman and Choueiri showed that under these constraints electrons near the magnetic reversal can experience significant drifts in the positive thrust direction, which may help maintain the charge neutrality of the exhausted plasma.

However, while single particle dynamics for both ions and electrons have been explored numerically and analytically, the interactions between the species have so far been ignored. In particular, while electrostatic waves have the ability to generate significant ion motion in the positive-$\hat{x}$ (thrust) direction, these same waves have little effect on electron motion. Therefore, electrons need to be pulled across field lines by the ions in order to maintain charge neutrality. Previous work on single-particle dynamics[1,10,11] lacks self-consistency because it does not address this need and the effect it has on ion motion and electron motion. Full analytical models which treat ions and electrons together have proven difficult to obtain, as the system must be treated kinetically due to the particle-null interaction. Consequently, we turn to numerical simulations to provide insight into the nature of the self-consistent particle dynamics. In this paper, we carry out a 2D proof-of-concept simulation of a plasma interacting with an externally applied magnetic reversal to demonstrate that this topology can induce net drift on a quasineutral plasma. These simulations are compared to the expected behavior of ions from the single-particle theory in order to show to what extent such a simplified theory can predict trends in the dependences of the relevant parameters. These simulations are performed using the LSP (Large Scale Plasma)[12] particle-in-cell (PIC) code.

In Section II, we review previous work on the magnetic null thruster, single particle dynamics, and how beating waves energize the plasma. In Section III, we describe the numerical set-up and important parameters of the plasma being investigated. In Section IV, we derive the expected single-particle dynamics of our simulated system. In Section V, we present the results of our simulations, including comparisons to single particle theory. Finally, in Section V, we discuss the applicability of the simulations and the insights derived from them, as well as where they fall short.

II. The MagNul Thruster Concept

A. The basic concept

The basic concept behind the MagNul thruster is to use a magnetic field reversal in order to achieve directed ion acceleration. The physics are most easily seen in a two-dimensional $\hat{x}\hat{y}$-plane with a magnetic field acting only in the $\hat{z}$-direction as show in Figure 2. In the upper half-plane, there is a uniform and constant magnetic field pointing in the positive-$\hat{z}$ direction. In the lower half-plane, an equal in magnitude field points in the opposite direction. In the immediate region near the the $y = 0$ plane, a magnetic reversal occurs generating the eponymous magnetic null. This region can be used to direct ions with appropriate sized gyro orbits

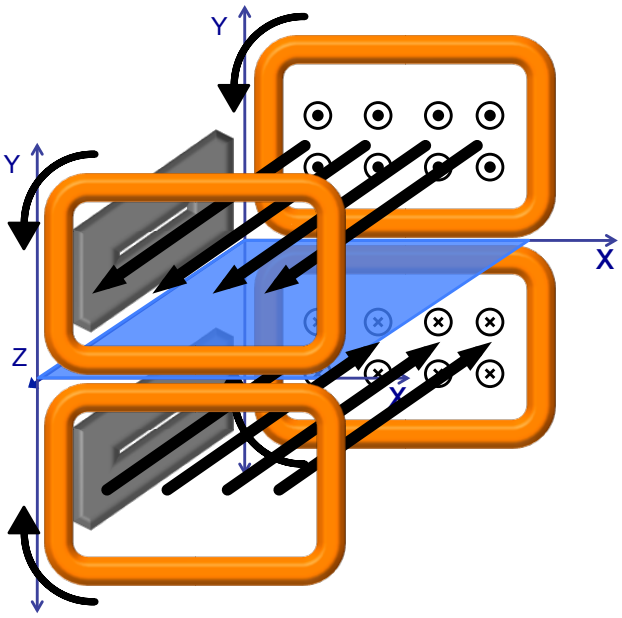

Figure 1. Schematic of the MagNul Thruster Concept. Current conducting Helmholtz-like coils, depicted in orange both above and below the $y = 0$ plane, create a magnetic field topology with a magnetic null shown in blue at the $y = 0$ plane. Beating electrostatic waves are launched from the black antennas at the $x = 0$ plane. The thrust is in the positive-$\hat{x}$ direction.

in the positive-$\hat{x}$ direction out of the thruster. Because ions in each half-plane orbit in opposite directions, those ions which cross the null are able to experience forward drifting linear betatron orbits.[1,13] Figure 2 illustrates this effect.

It is important to note that the null does not impart additional energy into ions. Rather, the MagNul thruster is intended to be powered by beating electrostatic waves. Electrostatic waves[2,3,5] have the ability to both accelerate and energize individual ions as well as drive them towards the region of magnetic reversal,[1,10] where they can be directed out of the thruster. Beating electrostatic waves in particular have been well explored previously[4,6,7] and are chosen because they can target and accelerate a larger fraction of the ion population than a single electrostatic wave. Together, beating electrostatic waves and the magnetic null topology have the potential to generate significant ion motion in the postive-$\hat{x}$ direction.[10]

A full three-dimensional illustration of one possible MagNul thruster configuration is shown in Figure 1. Two sets of Helmholtz-like field coils generate magnetic fields in opposite directions about the null-plane, and beating electrostatic waves can be launched in the positive-$\hat{x}$ direction from the antennas along the $x = 0$ plane both above and below the null.

B. Single Particle Dynamics

Previous work on the beating electrostatic wave powered MagNul thruster has focused on single particle motion of both ions and electrons in and around the magnetic reversal. Jorns and Choueiri[1] explored ion orbits analytically and characterized the Hamiltonian governing the equations of motion for an individual ion:

$$h = \frac{1}{2m}(\mathbf{p} - q\mathbf{A})^2, \tag{1}$$

where $\mathbf{p}$ is the canonical momentum, q is the electric charge of the particle, and $\mathbf{A}$ is the magnetic vector potential. In order to generate a magnetic reversal with characteristic size δ, Jorns and Choueiri assumed the following form for the vector potential: $\mathbf{A} = A_x(y) = \frac{\delta}{3}B_0 \log\cosh\frac{3y}{\delta}$. We note that:

$$\delta \to 0, \mathbf{A} \to A_x(y) = -|y|. \tag{2}$$

To simplify our work with single particle analysis in Section IV, we nondimensionalize the Hamiltonian equations, in the same manner as was done in previous work on the MagNul thruster,[1,10,11] except that we

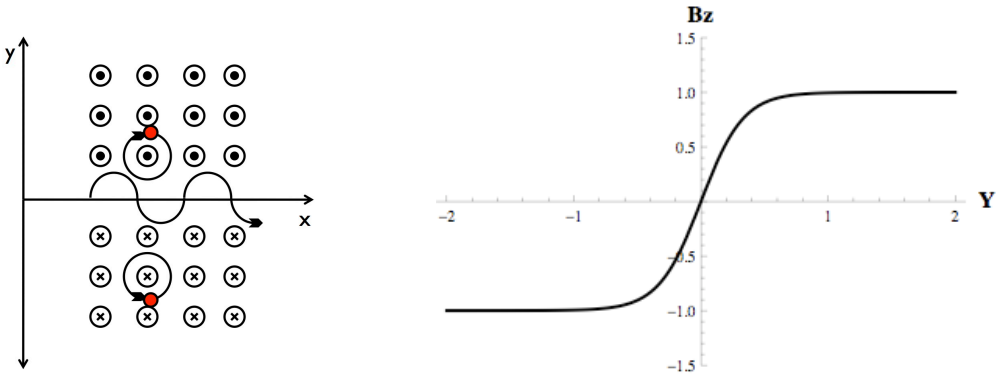

Figure 2. Magnetic Configuration. On the left, we see the Magnetic field has opposite polarity above and below the $\hat{x}$-axis. On the right, the Magnetic field, B_z normalized by B_0 is plotted against the normalized coordinate Y. Note that above $Y = 1$ the magnetic field is roughly uniform. This corresponds to the location where $y = \delta$.

normalize our length scale by ρ_{th}, the average Larmor radius for a Maxwellian distribution of ions with a given temperature, so that

$$H = \frac{1}{2}\left(\left[P_X - \bar{A}_X\right]^2 + P_Y^2\right), \tag{3}$$

where

$$\tau = \omega_c t \qquad H = \tfrac{h}{m v_{th}^2} \qquad X = \tfrac{x}{\rho_{th}} \qquad Y = \tfrac{y}{\rho_{th}}$$

$$\bar{A}_X = \tfrac{q}{m v_{th}} A_x(\rho_{th} Y) \qquad P_X = \dot{X} + \bar{A}_X \qquad P_Y = \dot{Y} \qquad \rho_{th} = \tfrac{v_{th}}{\omega_c}$$

and where $\omega_c = |\frac{qB_0}{m}|$ is the particle cyclotron frequency and $\dot{}$ represents differentiation with respect to τ. We note that both the Hamiltonian, H, and the canonical $\hat{x}$-momentum, P_X, are constants of motion for an individual particle in the given magnetic topology not subjected to any external electric fields. These can be related to the normalized physical coordinates by:

$$H = \frac{1}{2}\bar{\rho}^2 \tag{4}$$

$$P_X = -Y_{gc}, \tag{5}$$

where $\bar{\rho}$ and Y_{gc} are the nondimensionalized Larmor radius and particle guiding center, respectively.

Jorns and Choueiri[1] identified four types of ion orbits that occur due to interaction with a non-ideal magnetic field reversal (i.e., one where the length scale of the field reversal is non-negligible compared to the size of the ion orbits): linear betatron, forward figure-8, reverse figure-8, grad-B. The linear betatron and forward figure-8 orbits drift in the positive-$\hat{x}$ direction, while the reverse figure-8 and grad-B trajectories drift backwards. These trajectories are dependent on the two constants of motion, H and P_X. In the MagNul thruster we aim to exploit the positive drifting orbits to generate axial ion motion in the positive-$\hat{x}$ direction, which means the backward drifting orbits are harmful for thrust generation. These reverse-drifting orbits arise only due to the non-ideal nature of the field reversal. If the magnetic field reversal occurs on a length scale much smaller than the ion orbit sizes, the fraction of ions experiencing harmful reverse orbits becomes negligible.

Feldman and Choueiri[11] similarly explored the electron dynamics, where the characteristic size of electrons gyro-radii was much smaller than null region. Because of this, most electrons that do interact with the field reversal experience these "reverse figure-8" and "grad-B" drifts. However, due to their negative charge, these orbits also drift in the positive-$\hat{x}$ direction. This lead to the following intuitive criterion for thruster design

$$\rho_{e_{th}} \ll \delta < \rho_{i_{th}}, \tag{6}$$

where δ is the characteristic length of the magnetic field reversal in the null region.

C. Beating Electrostatic Waves

As mentioned above, the addition of beating electrostatic waves serves two important functions in this thruster configuration, the most obvious of which is to energize the ions. This particle energization occurs through a non-resonant process, characterized by Spektor and Choueiri,[4] which can coherently increase the ion velocity until it reaches a threshold value. At this point, an ion has sufficient velocity that it can be subjected to vigorous acceleration by a resonant process where ions stochastically receive periodic "kicks" in energy.

The second function of BEWs is to direct ions from the large regions of uniform magnetic fields towards the magnetic null region. This process occurs due to the stochastic acceleration mechanism. While in the stochastic regime, as an ion's energy increases, it is pushed towards the $y = 0$ magnetic null.[1] Mathematically speaking, Jorns and Choueiri derived the following relationship between the ion guiding center of motion and the energy increase:[1]

$$\langle |y_{gc}| \rangle = |y_{gc_0}| - \frac{1}{2v_{ph}\omega_{ic}}\left(v_i^2 - v_{i0}^2\right), \tag{7}$$

where y_{gc_0} is the initial guiding center location, v_{ph} is the Beating Wave phase velocity, ω_{ic} is the ion cyclotron frequency, and v_{i0} is the ion threshold velocity, which is the velocity at which an ion begins to experience the stochastic mode. Clearly, as the ion velocity increases, its guiding center moves towards $y = 0$.

While Jorns and Choueiri characterized which ions can be targeted for direct acceleration via beating electrostatic waves,[1] further simulations by Gardineer, et al[10] have demonstrated that beating electrostatic waves can be used to generate significant *directed* ion acceleration with exit velocities of at least 10 km/s.

D. Self Consistency

Previous work[1,10,11] on the MagNul thruster has focused exclusively on single particle dynamics. While this has provided insight into the behavior of the proposed thruster, the analysis is not self-consistent, as it ignores the electrostatic interactions between the ion and electron ensembles, as well as the effect of propagating beating waves on the plasma as a whole. The rest of this paper seeks to address the first deficiency by numerically simulating a quasineutral plasma interacting with a magnetic null, in order to demonstrate that ions can pull electrons across the magnetic field without adversely harming the essence of their single particle trajectories.

III. Numerical Approach

The purpose of this paper is to demonstrate numerically that plasma subjected to an externally applied magnetic field reversal can be preferentially directed along the axis. In a sense, the magnetic null topology is a unique nozzle designed to convert ion Larmor motion into directed thrust. Because this motion is inherently directed perpendicularly to the magnetic field, one avoids the traditional "detachment" issues with magnetic nozzles where plasma tends to stay stuck to magnetic field lines.[15] However, our own 'detachment' question exists, which is "what losses do ions incur in order to self-consistently pull electrons with them across the magnetic field lines?"

While we cannot yet give a complete answer to this question, in order to address it, we run a series of numerical simulations using LSP (Large Scale Plasma),[12] which is a commercial software that has been used to investigate other plasma systems including magnetized plasma flows[14] and betatron orbits in FRCs.[13] The software itself is a Particle-in-Cell (PIC) code. This approach is necessary as the traditional fluid equations are unsuitable for the ion dynamics as they undergo their forward betatron orbits, which require a kinetic or particle description. Because these orbits experience a breakdown of the first adiabatic invariant and the fluid equations are derived by integration over particle gyro orbits, the result is a significant finite-Larmor effect which is the main effect under investigation. The is best addressed by preserving the full kinetic trajectories of individual particles.

While eventually, a large set of simulations will be required to cover a wide range of parameters, these first simulations serve as a proof-of-concept to demonstrate the feasibility of externally applied magnetic reversals generating directed plasma motion.

A. The Simulation

We set up the simulation as follows in two-dimensions in the $\hat{x}\hat{y}$-plane. First, two 2.5 cm conducting walls are placed 2 cm apart in the $\hat{y}$-dimension. An external magnetic field is then generated such that the upper half plane above $y = 0$ has a uniform magnetic field of positive B_0, while the lower half plane has a field of negative B_0. In order to ignore the effects of a significant null on ion motion in these proof-of-concept simulations, the magnetic reversal itself is generated over a length scale much smaller than typical ion orbit sizes will be. To simulate plasma entering from the $\hat{z}$ direction, as would be the case in the proposed experimental configuration in Figure 1, a plasma is filled volumetrically in the the center of the simulation region, straddling the magnetic null. The plasma is composed of electrons and 1 amu ions with $T_e = T_i = 3$eV. This is done in a 1 cm by .5 cm region as shown in Figure 3 at a fill rate of approximately 1.25×10^{13} m^{-3} per nanosecond, and the system is allowed to reach steady state. The solution is computed using LSP's electrostatic, implicit field solver.

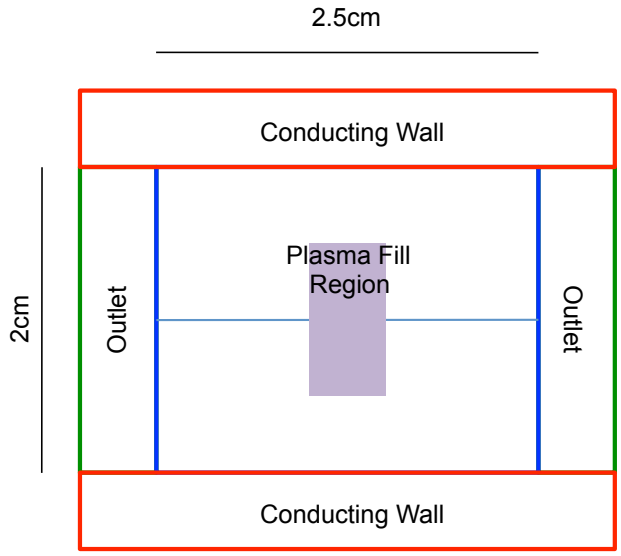

Figure 3. The 2D Space for the LSP simulations. The top and bottom red blocks are conducting walls located 2cm apart. The faint blue center line is the $y = 0$ magnetic null. Plasma is filled volumetrically in the center region about the null. The two blue vertical bars are the left and right outlets into non-conducting vacuum and are located 2.5cm apart.

The conducting walls serve to help confine the plasma in the absence of electrostatic waves, which would typically push the plasma towards the null. While argon is used for testing purposes in the beating electrostatic wave experiment,[8,9] protons are used here to increase our computational speed in these proof-of-concept simulations. Because the simulation time-step must resolve the electron cyclotron frequency and the simulation time-length is on the order of multiple ion cyclotron orbits, lighter ions allow us to make fewer total time steps in order to reach steady state. However, care must be taken to ensure the criterion laid out in Equation 6 is not violated, and that ion Larmor orbits remain much larger than electron orbits. This also allows us to utilize a smaller simulation space than argon would require for similar magnetic field strengths in the beating wave experiment, which operates at $B = 500$ G.

We preformed simulations for various magnetic field strengths from $B = 0$ G to $B = 800$ G. Given the ion mass and temperature, we can calculate the average ion Larmor radius over the full ensemble. These values are listed in Table 1.

In addition to typical simulation outputs for potential, particle number density and charge density, current density, and electric fields, we also record simulation results on the rate at which particles leave the system through each wall and each outlet, as well as the ion velocity distribution profiles over the entire thruster and at the positive and negative $\hat{x}$-outlets. This allows us to see how well the magnetic topology preforms at pushing the plasma in our preferred direction by calculating the flux rates of particles and momentum through the left and right outlets.

IV. Single Particle Comparison

Before presenting the results of our proof-of-concept simulations, we will re-examine single particle motion as applied to our particular simulation described above. This will give us a point of comparison for the self-consistent LSP simulations and help us determine what value the single particle approach may have for future analysis.

In our simulation, ions, with a 2D-Maxwellian velocity distribution, are loaded volumetrically in a region above and below the $y = 0$ magnetic null. If the ions satisfy the criterion $\rho_{th} \gg \delta$, the length scale of the reversal, which is the case in our simulation, we can approximate the null to be negligible in size. In this case, we note that all particles with $|P_X| < \sqrt{2H}$ will cross the null and be forward drifting.

In order to determine what fraction of particles are forward drifting, we must first transform the particle phase-space distribution into a distribution with respect to H and P_X. The normalized distribution function f_M is simply:

$$f_M(v_x, v_y, y) = \frac{1}{2y^*}\frac{m}{2\pi T_i}[\mathbf{H}(y + y^*) - \mathbf{H}(y - y^*)]e^{-\frac{m(v_x^2+v_y^2)}{2T_i}}, \tag{8}$$

where $\mathbf{H}$ is the Heaviside Step function, y^* is the height of the plasma fill above and below the magnetic reversal. Nondimensionally, we have:

$$F_M(u_X, u_Y, Y) = \frac{1}{Y^* 2\pi}[\mathbf{H}(Y) - \mathbf{H}(Y - Y^*)]e^{-\frac{1}{2}(u_X^2+u_Y^2)}, \tag{9}$$

where u is normalized by the ion thermal velocity, and, because of symmetry, we have altered the distribution function to only account for particles initially above the $y = 0$ null. Noting that

$$H = \tfrac{1}{2}(u_X^2 + u_Y^2) \qquad P_X = u_X - Y \qquad u_X = u\cos\theta \qquad u_Y = u\sin\theta,$$

we can easily transform the distribution into H-P_X-θ coordinates, and integrate out the θ coordinate, as it has no bearing on the shape of the orbit trajectory. Noting that the Jacobian of the coordinate transformation is unity, we find a new distribution

$$F(H, P_x, \theta) = \frac{1}{2\pi Y^*}[\mathbf{H}(\sqrt{2H}\cos\theta - P_X) - \mathbf{H}(\sqrt{2H}\cos\theta - P_X - Y^*)]e^{-H}. \tag{10}$$

$$F_{HP}(H, P_X) = \int_0^{2\pi} F(H, P_X, \theta)\, d\theta. \tag{11}$$

At this point, we introduce a new variable, S, which we define as

$$S = \frac{P_X}{\sqrt{2H}}. \tag{12}$$

Physically, S fully defines the shape of the trajectory of a particle crossing the null. If $S = 0$, an ion experiences very nearly semicircular orbits about the null. For $S = 1$, which the maximum value since P_X cannot be greater than $\sqrt{2H}$, a particle would be traveling perfectly along the $y = 0$ null in the positive-$\hat{x}$ direction. For $S < 1$, particles are no longer intersecting the magnetic reversal and instead are stuck in traditional Larmor orbits.

Coming back to our distribution function, clearly, the two Heaviside functions in F are unity when $\cos\theta > S$ and $\cos\theta > S + \frac{Y^*}{\sqrt{2H}}$, and 0 otherwise. When $S = 1$, no values of θ satisfy the first inequality. For any $S \leq -1$, all values of θ satisfy the inequality. However, since $\cos^{-1}$ is undefined for values less than -1, when we solve for θ, we see that $\theta_{step} = \cos^{-1}[\max(S, -1)]$ is the location of the step from zero to unity. A similar solution is generated for the second inequality, and since there are no other θ dependencies in our integration, we see that

$$F_{HP} = \frac{1}{\pi Y^*}e^{-H}\left[\cos^{-1}[\max(S, -1)] - \cos^{-1}[\max(S + \frac{Y^*}{\sqrt{2H}}, -1)]\right]. \tag{13}$$

Finally, we finish transforming our distribution into $H - S$ coordinates, and write our particle distribution function as

$$F_{HS} = \frac{\sqrt{2H}}{\pi Y^*}\left[\cos^{-1}[\max(S, -1)] - \cos^{-1}[\max(S + \frac{Y^*}{\sqrt{2H}}, -1)]\right]e^{-H}. \tag{14}$$

In this formulation, it is clear to see that particles that intersect the null are those with $|S| < 1$. Thus, in order to determine what fraction of the ion ensemble is in forward drifting orbits, we simply integrate within those limits:

$$\text{frac} = \int_0^\infty \int_{-1}^{1} F_{HS}\, dS\, dH. \tag{15}$$

We have so far neglected to exclude those particles which would be forward drifting but instead clip the top and/or bottom walls. This is easily corrected for by recalling from Section II that in normalized coordinates $Y_{gc} = -P_X$ and $\bar{\rho} = \sqrt{2H}$. Therefore, the maximum particle height allowed is given by $Y_{\max} = -S\sqrt{2H} + \sqrt{2H}$. When this is greater than the wall position, Y_W, a particle will clip the conducting wall. In order to exclude wall losses from our forward drifting calculation, we note that S must satisfy

$$S > 1 - \frac{Y_W}{\sqrt{2H}}. \tag{16}$$

We now can note that our new fraction of forward drifting particles is purely a function of Y^* and Y_W.

$$\text{frac} = \int_0^\infty \int_{\max\left(-1, 1-Y_W/\sqrt{2H}\right)}^{1} F_{HS}\, dS\, dH. \tag{17}$$

At this point, in order to calculate expected value of positive-$\hat{x}$ directed momentum for the particle ensemble, all we need is an expression for the particle drift velocities as a function of H and S . This non-dimensionalized drift velocity is easy to calculate by noting that the normalized larmor radius is $\bar{\rho} = \sqrt{2H}$ and the normalized guiding center location is $Y_{gc} = -P_X$. A particle trajectory is shown in Figure 4. The drift velocity is simply calculated as the normalized distance from the first point of intersection with the magnetic null to the second point, divided by the normalized time it takes to complete that fraction of the full particle orbit. Thus

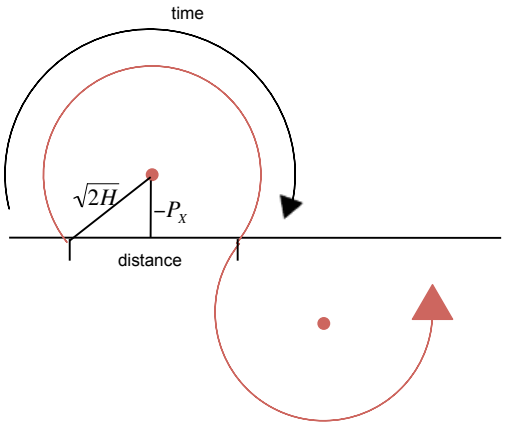

Figure 4. Particle undergoing Figure-8 drift with Hamiltonian H, and Canonical $\hat{x}$-momentum P_X. The non-dimensionalized distance traveled between two intersections of the magnetic null is $2\sqrt{2H - P_X^2}$. The non-dimensionalized time to get between the two intersections is proportional to the fraction of a full circular orbit and is $2\left[\pi - \cos^{-1}(-P_X/\sqrt{2H})\right]$.

$$u_d = \frac{2(2H - P_X^2)^{1/2}}{2\pi - 2\cos^{-1}(-\frac{P_X}{\sqrt{2H}})}, \tag{18}$$

or more simply:

$$u_d(H, S) = \sqrt{2H}\frac{(1 - S^2)^{1/2}}{\pi - \cos^{-1}(-S)}. \tag{19}$$

Armed with a particle distribution function and an equation for drift velocity, we calculate the expected $\hat{x}$-directed momentum for an ensemble of particles loaded into our simulation region. Non-dimensionalized

$\hat{x}$-momentum is simply $\bar{p}_x = \frac{mv_d}{mv_{th}} = u_d$. Therefore, the expected value of $\hat{x}$-directed momentum per particle is also a function of Y^* and Y_W and is:

$$< \bar{p}_x >= \int_0^\infty \int_{\max\limits_{(-1,1-\frac{Y_W}{\sqrt{2H}})}}^1 u_d(H,S)\ F_{HS}(H,S,Y^*)\ dS\, dH. \tag{20}$$

In our simulations, the fill height, y^*, is always 5mm and the wall height, y_W, is always 10mm, but as the B-field is increases, the non-dimensionalized Y^* and Y_W increase. These nondimensionalized parameters change between each simulation and are given below in Table 1.

B_0 (G)	$\rho_{i_{th}}$ (mm)	Y^*	Y_W
0	N/A	N/A	N/A
100	17.63	0.284	0.57
200	8.82	0.57	1.13
400	4.41	1.13	2.27
600	2.94	1.70	3.40
800	2.20	2.27	4.53

Table 1. Different magnetic field strengths used in LSP simulations, their corresponding average ion Larmor radius for a thermal ion ensemble at $T_i = 3$eV and $M_i = 1$amu, and Y^* of the corresponding distribution functions.

V. Numerical Results

The proof-of-concept numerical simulations were performed for magnetic field strengths varying from 0 G to 800 G. Each simulation was allowed to reach steady state. Our primary diagnostic tool for analyzing the steady-state behavior are probes measuring the ion $\hat{x}$-velocity distribution function near the right and left outlets. When combined with the ion densities at these exits, we are able to calculate particle and momentum fluxes, which can be compared to the expected single particle theory.

A. Ion Densities in Steady State

Before comparing our results with the single particle theory, we will look at the ion densities for a few different magnetic field strengths. These are shown in Figures 5-7. Electron densities are not shown, but quasineutrality is preserved in the simulation except in the sheath near the boundaries. The images in Figures 5-7 are for each system at B=200 G, 400 G, 600 G respectively, once it has reached steady state. For magnetic field strengths much smaller than 200 G, we can see from Table 1 that the typical ion Larmor orbit size becomes larger than the size of the system.

The most obvious feature in these runs is that the density along the magnetic null is distinctly less than the areas between the null and the confining walls. From a single particle treatment of ions in the magnetic topology, this is the region where most ions are experiencing forward drifts, and these ions typically experience faster drifts than those with larger values of $|y_{gc}|$. The net result is that the ions filling this region do not build up in steady state. Thus, this region with decreased density is in agreement with our expectation that some ions are maintaining their single particle orbits. We can also see that ion densities are greater near the right outlet as compared with the left outlet. While particles do still exit to the left outlet and to the conducting walls, the tendency to see higher densities towards the right outlet suggests that the plasma is being preferentially directed by the null as desired. To ensure this, we also need to calculate the particle flux rates, which is done in Section V.B.

B. Particle and Momentum Fluxes

The primary data we recorded through our simulations were the $\hat{x}$-velocity distributions of ions within 2mm of the simulation outlets. Combined with the average densities in this region, we can integrate over the distribution in order to determine the particle flux and momentum flux through both outlets. The velocity

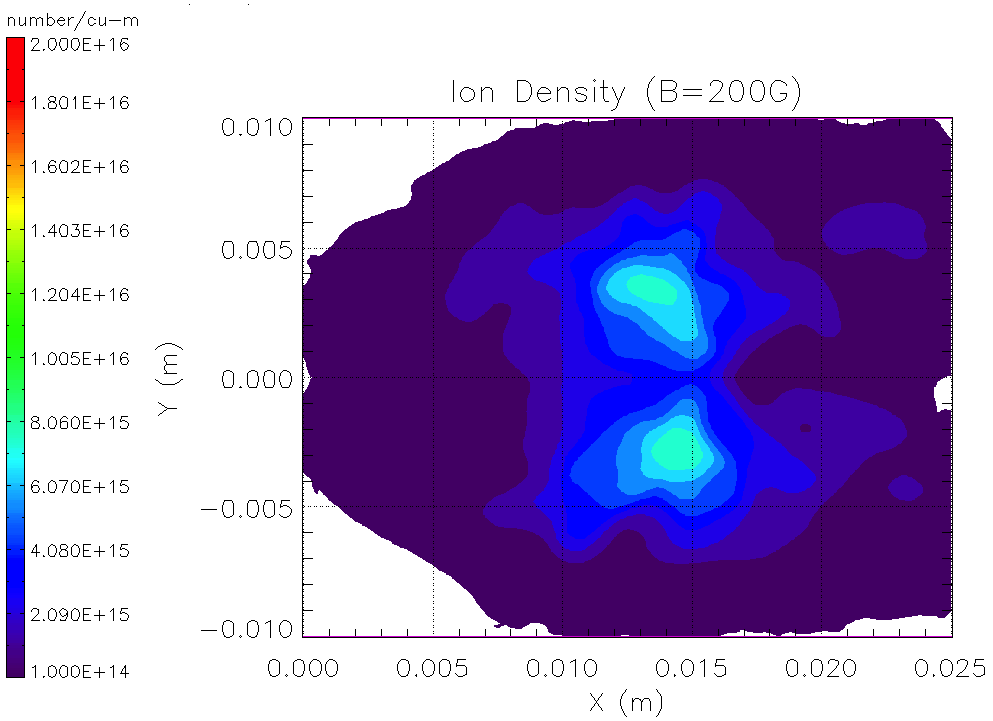

Figure 5. Steady-state density plot of ion density for a magnetic field strength of 200 G ($Y^* = .567$)

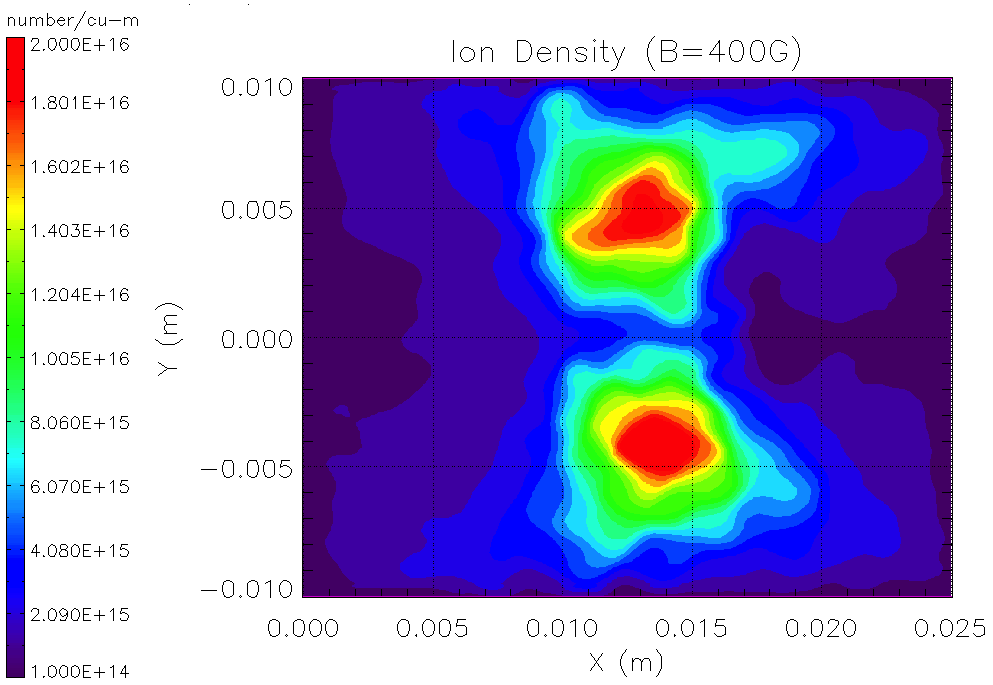

Figure 6. Steady-state density plot of ion density for a magnetic field strength of 400 G ($Y^* = 1.134$)

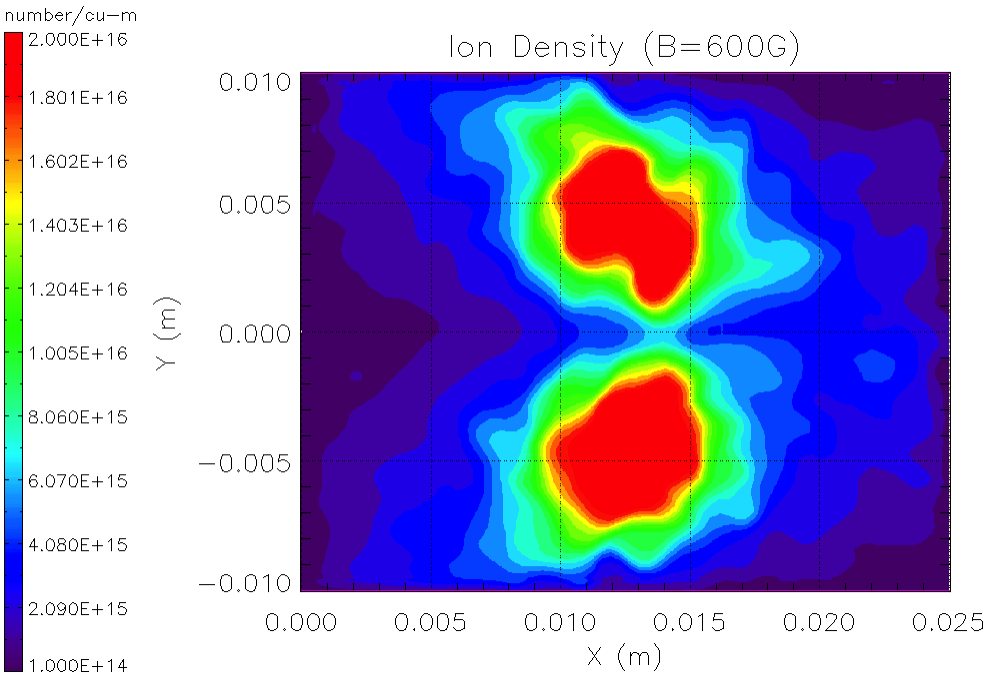

Figure 7. Steady-state density plot of ion density for a magnetic field strength of 600 G ($Y^* = 1.701$)

distributions for the right outlet and left outlet are shown in Figures 8 and 9 and were taken once the system had reached steady state.

In order to calculate the particle flux rate through the right boundary of a simulation, we must simply integrate over the right side $\hat{x}$-velocity distribution:

$$\frac{\#\,\text{particles}}{\text{meter sec}} = \int\int nvf_r(v)dvdA. \tag{21}$$

Since our simulation is only in two-dimensions, the area we integrate over is only the simulation height, $y = 2cm$, which results in a flux-rate per length in the non-simulated $\hat{z}$-direction.

In order to compare this to our single particle calculations in Section IV, we also must know the rate of particles entering the simulation (per meter in the $\hat{z}$-direction). Since our volumetric fill rate is $1.25 \times 10^{13}\,\text{m}^{-3}/\,\text{ns}$, and the two-dimensional fill area is 1 cm x.5 cm, we have a fill rate of $R = 6.25{\times}10^{17}$ ions/(meter sec). The fill rate is used to normalize our calculated particle fluxes, which gives us the fraction of the particles which efflux out of the right outlet. A similar calculate can be made for the particle flux in the backwards direction through the left outlet. This calculation is made for each simulation and plotted in Figure 10 along with the expected results from the single particle theory described in Section IV.

The important takeaway from Figure 10 is that over our parameter range of magnetic fields, we see the magnetic topology does generate net motion of particles primarily in our preferred positive-$\hat{x}$ direction. We also note that the fraction of particles which exit forward is much less than predicted by single particle theory. These particles are being lost primarily to our confining conducting walls. Essentially, the predicted single-particle motion of individual ions is being hampered by the self-consistent effects required to maintain charge balance. However, while a large fraction of particles are being lost to the walls of the system, we expect the addition of beating electrostatic waves to channel more ions towards the magnetic reversal and away from the walls, which should result in a larger fraction of particles exhausting in the forward direction.

Moreover, though the single particle theory does seem to predict the optimum value of Y^*, where the net particle flux is maximized.

We can preform a similar integration for at the right and left outlets in order to calculate the momentum flux in the positive and negative $\hat{x}$-directions through each outlet.

$$\frac{\text{momentum}}{\text{meter sec}} = \int\int mnv^2 f_r(v)dvdA \tag{22}$$

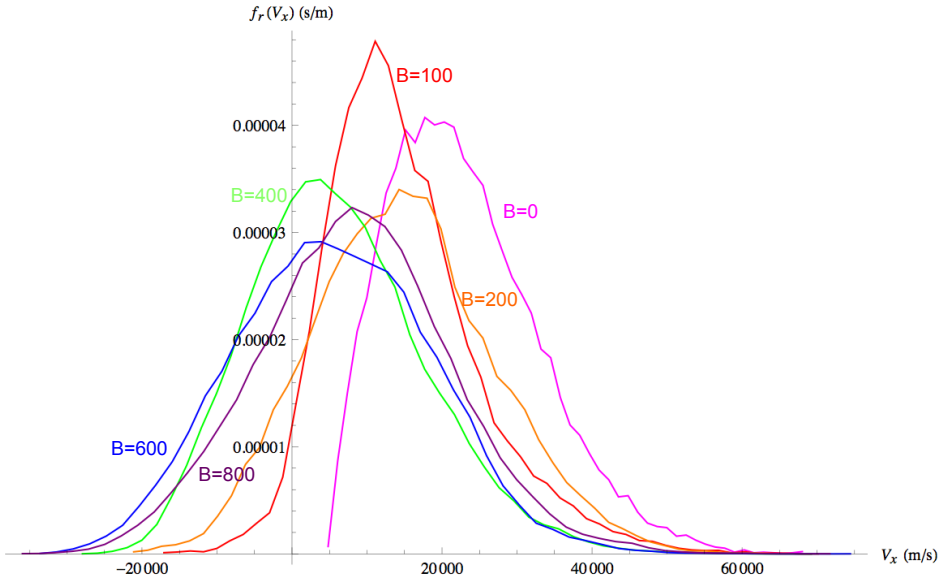

Figure 8. Distributions of velocity in the $\hat{x}$-direction near the right outlet. We can see visually that as the magnetic field strength increases, the peak velocity distribution shifts closer to $v_x = 0$. These distributions can be integrated over in order to obtain particle and momentum flux through the right-side outlet.

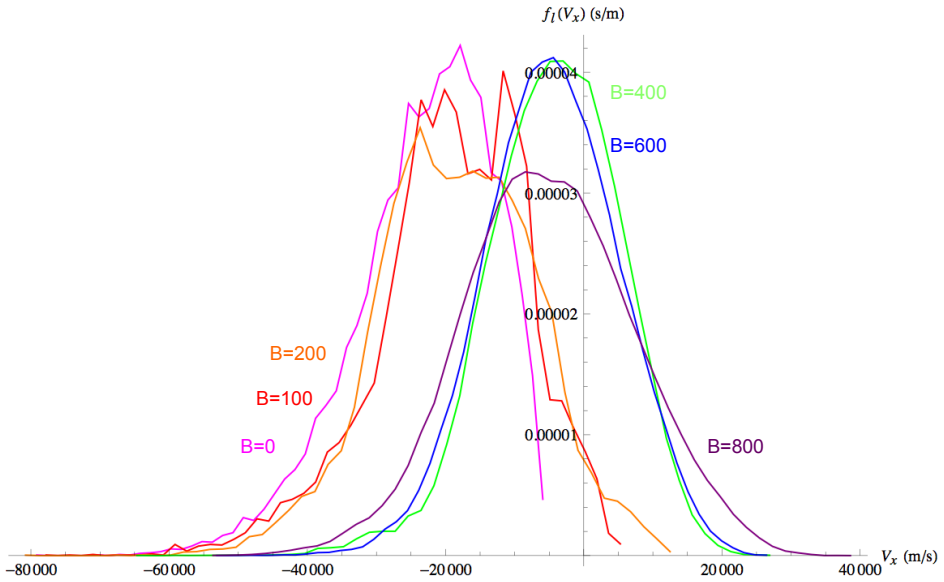

Figure 9. Distributions of velocity in the $\hat{x}$-direction near the left outlet. We can see visually that as the magnetic field strength increases, the peak velocity distribution shifts closer to $v_x = 0$. These distributions can be integrated over in order to obtain particle and momentum flux through the left-side outlet.

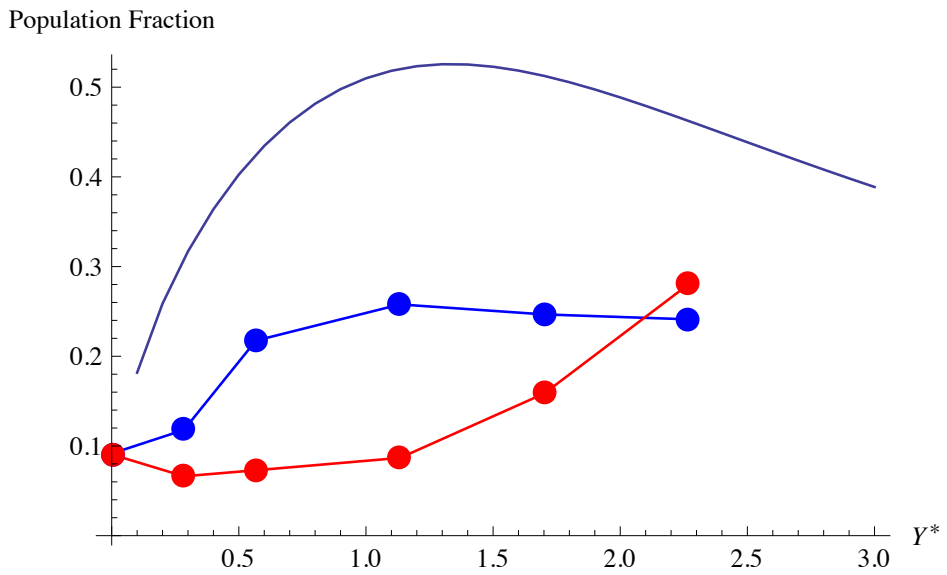

Figure 10. Fraction of particle population exiting the two outlets and expected forward drifting fraction from single-particle theory. The blue dots are the simulated data for particle fraction exiting the right (i.e., forward) outlet of the simulation corresponding to $B = 0, 100, 200, 400, 600$ G consecutively with increasing Y^*. The red dots represent the simulated particle fraction exiting left (i.e., backwards). The solid line is the forward drifting fraction predicted from single particle theory.

We again normalize the calculated momentum flux values by the rate of particles and momentum entering the system and compare to the predictions from single-particle theory. A plot of the normalized forward and reverse momentum, along with the single particle forward momentum prediction, is shown in Figure 11.

Because the momentum which effluxes through the right (i.e. forward) outlet is distinctly larger than the momentum flux in the reverse direction, it is clear that a net momentum is imparted to the plasma by the magnetic null topology. That is, the magnetic reversal generates thrust by directing particle motion primarily in our preferred direction!

Once more, we note that the momentum calculated is less than the expected forward momentum imparted from single particle theory. Interestingly, while the net particle flux is much lower than expected, the net momentum flux seems to match more closely to the single particle predictions. This implies that the particles "lost" to the conducting walls are those that were not carrying a significant portion of the $\hat{x}$-directed momentum. This makes intuitive sense, as the particles closest to the walls and most easily lost are less likely to have large drift velocities than those particles nearer to the magnetic null. Therefore, we expect them to be carrying a smaller fraction of the momentum and the resultant momentum loss to be less severe.

The MagNul thruster concept relies heavily on the idealized motion of ions within the magnetic topology. If ions cannot be expected to maintain the essence of these trajectories while self-consistently pulling electrons, the usefulness of the concept as a propulsion device would be called into question. If ions can be expected to follow these single particle predictions, this suggests that the single particle analysis may serve as a guide to help optimize thruster performance in some situations. Fortunately, in our limited data set, we do see an agreement in trends between the simulated and calculated values; though it is clear that we do not get as much momentum generation as the single-particle theory predicts. Most importantly, the single particle theory does appear to predict the optimum magnetic field strength, which suggests it could be used in future analysis to help tune thruster performance. However, it is clear that a larger parameter space should be explored in order to determine when the idealized single-particle trajectory calculations can be applied to give us useful insights.

VI. Discussion and Concluding Remarks

In this paper, we presented the first self-consistent simulations of ion-electron behavior in an externally applied magnetic field reversal by utilizing a PIC code and allowing the system to reach steady state. Using

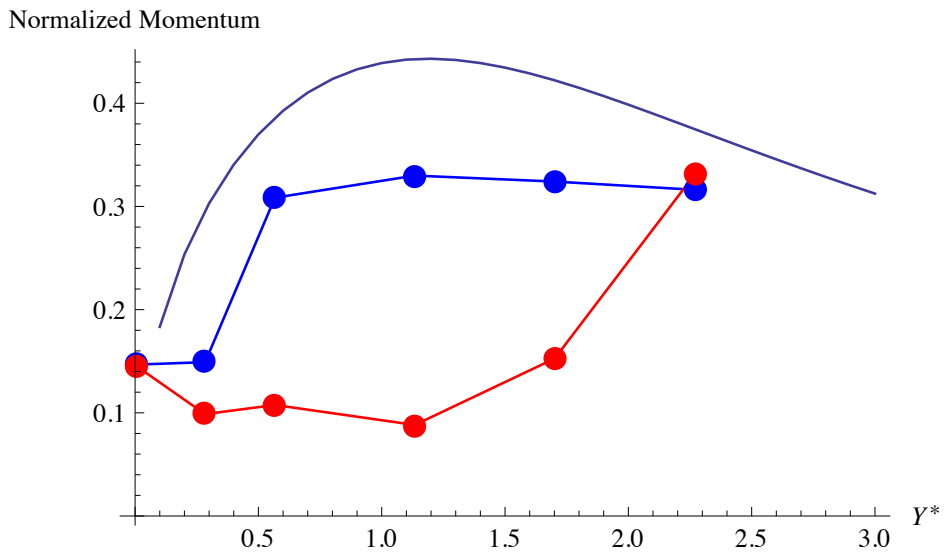

Figure 11. Normalized momentum exiting the two outlets and expected momentum from single-particle theory. The blue dots are the simulated data for normalized momentum exiting the right (i.e., forward) outlet of the simulation corresponding to $B = 0, 100, 200, 400, 600$ G consecutively with increasing Y^*. The red dots represent the simulated momentum exiting left (i.e., backwards). The solid line is the forward momentum predicted from single particle theory.

the velocity distribution profiles near the forward and reverse outlets of the simulation space, particle and momentum fluxes were calculated, demonstrating that the directed motion of a quasineutral plasma can be achieved with a magnetic null topology. The particle and momentum fluxes were also compared with single particle theory for ions in an 'ideal' null topology. While the results did not match quantitatively, the agreement in trends between the single particle theory and the self-consistent particle simulation suggests that the former may give us insight into the behavior, scaling, and optimization of the thruster. However, we note that more of the parameter space (including varying magnetic field strength, ion mass, and particle density) needs to be explored in order to determine when this approximation can be safely applied.

We also observed a significant loss of particles to the upper and lower conducting walls in our simulations. This is not entirely surprising, as many particles remain trapped in non-drifting Larmor orbits and eventually are pushed out of the simulation through collisions and intersection with the sheath near the conducting walls. While this may seem disconcerting at first, it is important to note that the addition of electrostatic waves will serve to confine the plasma by channeling ions towards the magnetic null. As a result, we do not expect to see such significant particle losses in a fully integrated thruster.

Additionally, our single-particle theory and LSP simulations suggests an optimal magnetic field strength exists, where the MagNul topology directs the largest portion of the plasma momentum forward. This optimum occurs when the plasma fill heigh, y_f, is roughly equal to the typical ion Larmor orbit size, ρ_{ith}. In words, the ion Larmor size must not be too small, or not enough ions will experience forward drifting orbits, but they also cannot be too large, as those ions will be lost the the thruster walls.

We realize that these first proof-of-concept simulations were performed over a limited section of the parameter space with lower densities and a different ion mass than one might typically see in a beating electrostatic wave plasma.[6,7] Further study is required to explore the full parameter space of plasma interacting with an externally applied magnetic field reversal, in order to determine the extent of the capabilities of the magnetic null topology.

Acknowledgments

This research was carried out with support from the Plasma Science and Technology Program from the Princeton Plasma Physics Laboratory. The authors would like to acknowledge Dr. Dale R. Welch for helpful information regarding the LSP[12] code.

References

[1]Jorns, B. and Choueiri, E.Y., "A Plasma Propulsion Concept Based on Direct Ion Acceleration with Beating Electrostatic Waves," 46^{th} Jnt. Prop. Conf. Number AIAA-2010-7107, July 2010.

[2]Benisti, D., Ram, A. K., and Bers, A., "Ion dynamics in multiple electrostatic waves in a magnetized plasma. I. Coherent acceleration," Physics of Plasmas, Vol. 5, No. 9, 1998, pp. 3224-3232.

[3]Benisti, D., Ram, A. K., and Bers, A., "Ion dynamics in multiple electrostatic waves in a magnetized plasma. II. Enhancement of the acceleration," Physics of Plasmas, Vol. 5, No. 9, 1998, pp. 3233-3241.

[4]Spektor, R. and Choueiri, E. Y., "Ion acceleration by beating electrostatic waves: Domain of allowed acceleration," *Physical Review E*, Vol. 69, No. 4, April 2004, pp. 046402.

[5]Karney, C. and Bers, A., "Stochastic Ion Heating by a Perpendicularly Propagating Electrostatic Wave," *Physical Review Letters*, Vol. 39, No. 9, 1977, pp. 550.

[6]Jorns, B., Choueiri, E.Y., "Efficiency of Plasma Heating with Beating Electrostatic Waves," 47^{th} Jnt. Prop. Conf. Number AIAA-2011-5894. July 31- Aug 3, 2011.

[7]Jorns, B. and Choueiri, E.Y., "Ion Heating with Beating Electrostatic Waves," *Physical Review Letters*, Vol. 106, No. 8, Feb. 2011.

[8]Jorns, B. and Choueiri, E.Y., "Experiment for Plasma Energization with Beating Electrostatic Waves," 31^{st} International Electric Propulsion Conference. IEPC-09-199. Sep 21 - 24, 2009.

[9]Jorns, B. and Choueiri, E.Y., "Experimental Characterization of Plasma Heating with Beating Electrostatic Waves," 48^{th} Jnt. Prop. Conf. Number AIAA-2012-4194. July 30 - Aug 1, 2012.

[10]Gardineer, B., Jorns, B., Choueiri, E.Y., "Simulations of Direct Ion Acceleration with Beating Electrostatic Waves," 32^{nd} Int. Elec. Prop. Conf., Number IEPC-2011-212, September 2011.

[11]Feldman, M.S., Choueiri, E.Y., "Electron Dynamics in a Beating Electrostatic Wave Magnetic Null Thruster," 48^{th} Jnt. Prop. Conf. Number AIAA-2012-4193. July 30 - Aug 1, 2012.

[12]LSP is a software product developed by ATK Mission Research, Albuquerque, NM 87110.

[13]Welch, D.R., Cohen, S.A., Genoni, T.C., Glasser, A.H., "Formation of Field-Reversed-Configuration plasma with Punctuated-Betatron-Orbit Electrons," *Physical Review Letters*, 105,015002. (2010).

[14]Sefkow, A.B., Cohen, S.A., "Particle-in-Cell Modeling of Magnetized Argon Plasma Flow through small Mechanical Apertures," *Physics of Plasmas*, 16,053501. (2009).

[15]Little, J.M., Choueiri, E.Y., "Plasma Detachment and Momentum Transfer in Magnetic Nozzles," 47^{th} Jnt. Prop. Conf. Number AIAA-2011-6001. July 31 Aug 3, 2011.